RESEARCH PAPER

Channels 9:5, 324–333; September/October 2015; Published with license by Taylor & Francis Group, LLC

Single calcium channel domain gating of synaptic vesicle fusion at fast synapses; analysis by graphic modeling

Elise F Stanley*

Toronto Western Research Institute; Toronto, Ontario Canada

Keywords: calcium channel, microdomain, nanodomain, overlapping domain, presynaptic, single domain, single channel synaptic vesicle, transmitter release

At fast-transmitting presynaptic terminals Ca^{2+} enter through voltage gated calcium channels (CaVs) and bind to a synaptic vesicle (SV) -associated calcium sensor (SV-sensor) to gate fusion and discharge. An open CaV generates a high-concentration plume, or nanodomain of Ca^{2+} that dissipates precipitously with distance from the pore. At most fast synapses, such as the frog neuromuscular junction (NMJ), the SV sensors are located sufficiently close to individual CaVs to be gated by single nanodomains. However, at others, such as the mature rodent calyx of Held (calyx of Held), the physiology is more complex with evidence that CaVs that are both close and distant from the SV sensor and it is argued that release is gated primarily by the overlapping Ca^{2+} nanodomains from many CaVs. We devised a 'graphic modeling' method to sum Ca^{2+} from individual CaVs located at varying distances from the SV-sensor to determine the SV release probability and also the fraction of that probability that can be attributed to single domain gating. This method was applied first to simplified, low and high CaV density model release sites and then to published data on the contrasting frog NMJ and the rodent calyx of Held native synapses. We report 3 main predictions: the SV-sensor is positioned very close to the point at which the SV fuses with the membrane; single domain-release gating predominates even at synapses where the SV abuts a large cluster of CaVs, and even relatively remote CaVs can contribute significantly to single domain-based gating.

Introduction

Fast information transfer between neurons and their target cells occurs at classical chemical synapses where release-ready, transmitter-filled synaptic vesicles (SVs) dock to the presynaptic terminal surface membrane opposite target receptors on the post-synaptic cell. Action potentials open voltage sensitive calcium channels (CaVs) to admit extracellular Ca^{2+} which diffuses to, and bind to an SV calcium-sensor (SV-sensor), triggering fusion and transmitter discharge. To minimize random ambient cytoplasmic Ca^{2+}-triggered SV discharge, activation of the SV-sensors requires the simultaneous binding of multiple (n) Ca^{2+} (typically with $n = 4$ or 5[1-3]; herein $n = 5$) to relatively low-affinity binding sites.[3,4] Thus, action potential-triggered gating of SV fusion requires a substantial increase of local Ca^{2+} from resting levels.[4-7] Due to a number of factors, in particular activation of only a fraction of the transmitter release face CaVs (open probability = Po), each action potential typically triggers the release of only a subset of the docked and 'release-ready' SVs. The ratio of released to release-ready SVs is defined as the ***release probability*** (P_R), a value that is characteristic for a particular synapse type.[8]

The finding of a very short, 0.2 ms minimal latency between Ca^{2+} entry and SV discharge, during which the ions could only diffuse ~100 nm, led to the prediction that the CaVs must be located very close to the SV sensors.[9] Further advance in the understanding of transmitter release physiology followed the realization that Ca^{2+} streaming in through an open channel creates a standing 'plume' of ions centered on the channel, now termed a *nanodomain*, with the Ca^{2+} concentration declines steeply from ~mM at the channel mouth to near resting Ca^{2+} levels a fraction of a μm away[10,11] (**Fig. 1**). Simple dispersion of the ions into the 3-dimensional cytoplasmic space is the main reason for the steep gradient, but this can be enhanced by cytoplasmic Ca^{2+} scavengers. Thus, local activation of release in the nerve terminal was attributed to the pooling of Ca^{2+} nanodomains from large CaV clusters, generating a 'Ca^{2+} microdomain' that overlapped and activated the SV-sensors.[5,12]

*Correspondence to: Elise F Stanley; Email: elise.f.stanley@gmail.com
Submitted: 09/08/2015; Revised: 09/14/2015; Accepted: 09/16/2015
http://dx.doi.org/10.1080/19336950.2015.1098793

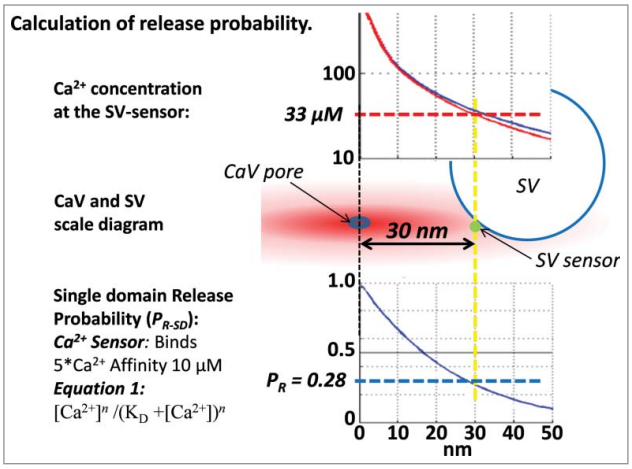

Figure 1. The central diagram shows an SV with its sensor 30 nm from the channel pore (*vertical yellow dashed line*). The concentration of Ca^{2+} at that distance can be read off the CaV nanodomain profile[30] (*red line*; used in all calculations unless stated; the nanodomain profile with 50 μM fixed buffer, *blue line*, is shown for comparison). The probability that the SV will fuse, calculated using the equilibrium binding equation (*lower left*; with 5 independent Ca^{2+} binding sites each with a 10 μM affinity[4]) is plotted at the lower right and predicts a release probability of 0.28 (*horizontal dashed blue line*).

Release site physiology underwent a further re-evaluation with the novel suggestion, based on the effect of reversible and irreversible channel blockers on transmitter release, that single CaV Ca^{2+} nanodomain might by itself saturate the SV-sensor Ca^{2+} binding sites to gate fusion.[13] This idea was supported by the finding at the squid giant synapse that transmitter release followed a linear function relative to the predicted recruitment of CaVs with increasing action potential durations[14] and was consistent with a resistance of release to slow on-rate Ca^{2+} scavengers (in particular EGTA; *see also below*).[15,16] Cell-attached recordings at a vertebrate calyx-type presynaptic terminal demonstrated that transmitter release remained time-locked with calcium current fluctuations even when the channels were opening one-at-a-time and provided compelling evidence that a single channel could indeed gate SV fusion.[17]

Two main experimental approaches have been devised to distinguish between overlapping and single domain-based release site gating. The first of these, termed here ***CaV-titration***, is, in essence, to vary the fraction of activated presynaptic calcium channels and plot this against the amplitude of transmitter release. If release is gated by Ca^{2+} pooling from remote CaVs the relationship is fit by a power function with an exponent of N, where $N = n$, (where n = the number of Ca^{2+} binding sites on the SV-sensor). At the other extreme, if SV release is gated by a CaV single domain then $N = 1$ (since the nanodomain saturates all the SV-sensor binding sites and hence, release is proportional to the number of recruited CaVs). The second method tests the sensitivity of transmitter release to a Ca^{2+} 'slow on-rate scavenger' introduced into the presynaptic cytoplasm. This scavenger has time to capture the incoming Ca^{2+} only if the CaVs are relatively remote from the SV-sensor.[15] The method is typically carried out with 10 mM EGTA in the intracellular buffer and is termed here the ***EGTA-sensitivity*** test. Briefly: the more sensitive transmission is to block by EGTA,[15] the stronger the argument for overlapping domains. Useful as these tests are, both are subject to assumptions.[18,19] Based primarily on these tests most studies have concluded that at fast-transmitting synapses single domain gating predominates.[20-25,26-29] However, as discussed below, if SVs are 'within range' of more than one simultaneously open CaV the release probability will exhibit a domain '*overlap bonus*'.

A number of studies have combined physiological analysis with mathematical modeling to explore the relationship between CaV domains and release. Until relatively recently these efforts have been limited by uncertainty with respect to the most important factor that determines nanodomain characteristics: the rate of Ca^{2+} ion influx through the CaV under physiological conditions. Ultra-low noise recording methods were used to determine this value for representative members all 3 CaV families, including CaV2, the family type that is predominant at presynaptic terminals.[30] The measured ion influx rate and an approximation of mobile cytoplasmic ion scavenger, ~50 μM of a 'fast' buffer,[31] was used to create a physiologically-tenable single channel nanodomain profile[30] (**Fig. 1**, *upper panel*). Based on this work we have devised a 'graphic modeling' method to model activation of transmitter release (specifically P_R) by virtually any architectural arrangement of CaVs and the SV-sensor target. Graphic modeling calculates the contribution of each individual CaV to the SV-sensor binding sites and, hence, the probability that the SV will fuse. To keep the method transparent and applicable between synapses we minimized the number of parameters as far as possible (*see* **Methods**). Graphic modeling was first applied to simplified architectures of CaV distribution including a minimal release site with one to 3 CaVs that abut the SV-sensor (see also[19,32]) and a maximized release site with a virtually crystalline array of channels radiate from the SV-sensor on the presynaptic membrane.

The graphic modeling method was then used to explore release gating at 2 contrasting biological synapses with detailed published data on release physiology and CaV distribution. At the frog NMJ the presynaptic terminal courses along the muscle fiber with numerous transverse release sites composed of 2 rows of docked vesicles separated by release apparatus that includes the CaVs.[33] Nanometer-resolution freeze fracture replicas reveal large particles arranged as 2 pairs of parallel rows[34] that have been attributed to CaVs[34-36] but recent findings argues that the active channels number only ~15% of the total particle number, comparable to the number of docked vesicles.[37,38] It is well established that single CaV gating predominates at this synapse[21,24,37,38] and key parameters have been measured including the CaV Po, 0.16,[37] and the P_R, 0.06.[38] These parameters, together with freeze-fracture quantification of the precise site where the SV fuses[39] were used to explore the location of the SV-sensor with respect to the channel and the SV fusion pore.

The method was then applied to the rodent calyx of Held, a synapse that serves as a relay for the transmission of high

Table 1. Release parameters for the calyx of Held

	Young Adult Calyx	Neonate Calyx
P_R	~0.2[#]	~0.1[#]
N[40]	$N < N_{MAX}$	$N = N_{MAX}$
EGTA[40]	20% block	55% block
N (EGTA)[40]	—	1 N_{MAX}

[#]see text
P_R, SV release probablity
N, CaV-titration test exponent
EGTA, Inhibition of release by 10 mM EGTA
N **(EGTA)**, CaV-titration exponent with 10 mM EGTA

frequency impulse trains in the auditory pathway. Both EGTA-block[40,41] and CaV-titration values (N)[40,42] are consistent with a significant single domain-contribution to release gating (**Table 1**).[40,41,43,44] Graphic modeling was carried out with various channel arrangements using the key parameters with CaV $Po = 0.2$ and $P_R = \sim 0.2$.[45-47] Numerous reports suggest that gating of release is very different at this synapse during development (herein 'Neonate Calyx of Held'), prior to functional transmission,[48] concluding that SV fusion is gated by overlapping domains from remote channels[41,42,49,50] (**Table 1**). Recently, CaV2.1 channels were localized by immunogold on calyx of Held presynaptic freeze-fracture replicas[51] and putative release sites exhibited an average of ~12 gold particles. Underlying SVs could not be imaged but, based on the EGTA block test, a modeling approach localized the SV sensor to ~19 nm from the nearest CaV. To attain the observed kinetics of release it was also concluded that the average release sites has a much larger, ~26 field of channels and that release was gated almost exclusively by overlapping Ca^{2+} domains.[52] We used graphic modeling to explore SV gating at the calyx of Held using the published release parameters. We find that if the SV is close to any individual CaV and the channel open probability is low, single domain-based SV gating should predominate over overlapping domains.

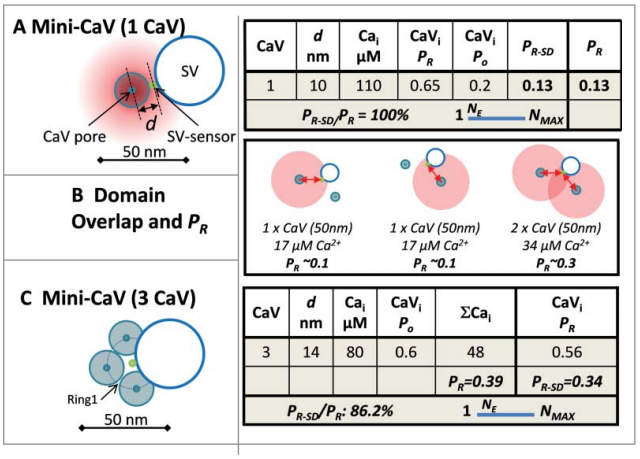

CaV	d nm	Ca_i μM	CaV_i P_R	CaV_i P_o	$P_{R\text{-}SD}$	P_R
1	10	110	0.65	0.2	0.13	0.13
$P_{R\text{-}SD}/P_R$ = 100%				1 N_E N_{MAX}		

CaV	d nm	Ca_i μM	CaV_i P_o	ΣCa_i	CaV_i P_R
3	14	80	0.6	48	0.56
				P_R=0.39	$P_{R\text{-}SD}$=0.34
$P_{R\text{-}SD}/P_R$: 86.2%				1 N_E N_{MAX}	

Figure 2. Minimal release site. (A) *Calculation of the release probability with a single CaV.* The diagram shows a release site with the SV abutting a single CaV with its sensor 10 nm (*d*) from the channel pore (*all diagrams are depicted viewing from the synaptic space, through the surface membrane and into the nerve terminal*). The worksheet summarizes the Ca^{2+} concentration seen by the SV-sensor (Ca_i); the release probability of an open channel (CaV_i, P_o); the number of open channels with P_o = 0.2 (CaV_i * P_o), and the overall release probability (P_R) calculated as in **Fig. 1**. The estimated CaV-titration N value (N_E) is diagramed on a slider between the minimum possible value, 1, and the maximum value for that synapse (*see text*). (**B**) *Two CaVs, equidistant from the SV-sensor.* Note the P_R in the overlapping domain is greater than the sum of the 2 single nanodomains providing an 'overlap-bonus' (*worksheet not shown*). (**C**) *Three CaVs located equidistant from the SV sensor.* Worksheet as in A, but with 2 release probabilities: P_R, calculated from the pooled Ca^{2+} (CaV^*-Ca_i), and $P_{R\text{-}SD}$ the sum of the probabilities that the Ca_i from each single channel will activate the SV-sensor.

Results

Graphic modeling estimation of release probabilities

Graphic modeling is a method devised to estimate the overall release probability (defined as probability that the SV-sensor Ca^{2+} binding sites are saturated), P_R, and also the fraction of P_R that can be attributed to single CaV domains, $P_{R\text{-}SD}$. P_R is calculated by determining the sum total of Ca^{2+} at the SV-sensor pooled from each open channel and calculating the probability of SV-sensor activation (see **Methods**, **Fig. 1**). $P_{R\text{-}SD}$ is calculated by determining the probability that any individual CaV will activate the SV-sensor and summing these probabilities (**Fig. 2A, C**). The $P_{R\text{-}SD}/P_R$ ratio (expressed as a percentage) is taken as the fraction of release that can be attributed to single domains with the residual due to overlapping domains. This ratio is related inversely to the CaV-titration, N value (see **Introduction**). N must lie in the $1 \leq N \leq N_{MAX}$ range (where $N_{MAX} = n$, the number of SV sensor Ca^{2+} binding sites). Thus, if $P_{R\text{-}SD}/P_R = 0\%$, transmitter release is gated entirely by a microdomain of Ca^{2+} from remote channels and $N = N_{MAX}$, while if $P_{R\text{-}SD}/P_R = 100\%$, release is gated by individual CaV nanodomains and $N = 1$. While we cannot calculate the precise value of N for a particular simulation, for the purpose of discussion its estimated value (N_E) is shown on a linear sliding scale ranging from 1 to N_{MAX} (e.g. **Figs. 2A, 2C, 3A**).

Minimal calcium channel density release sites

The simplest release site organization comprises a single CaV abutting the SV sensor (**Mini-CaV; Fig. 2A**).[53] If we assume that the SV-sensor does not overlap the CaV then the radius of the channel, ~10 nm (see **Methods** for dimensions), is a reasonable minimal distance between these elements. Based on our channel domain concentration profile, at this distance the SV sensor is exposed to 110 μM Ca^{2+}, predicting (**Fig. 1C**) an SV-sensor activation probability of 0.65 (**Figs. 1, 2A** *worksheets*). Using a CaV open probability of 0.2,[54] the probability of SV-sensor (with $n = 5$) activation, P_R, is 0.13. As there is only one channel the calculated P_R value is also the single-domain release probability, $P_{R\text{-}SD}$ and the $P_{R\text{-}SD}/P_R$ ratio is 100% and $N_E = 1$.

With a second channel there are 3 different ways of activating the SV-sensor: by each channel alone (**Fig. 2B**, *left 2 panels*), or by the overlapping domain of Ca^{2+} if both channels open (**Fig. 2B**, *right panel*).[32] Because of the curved relationship

A. Maxi-CaV Release site

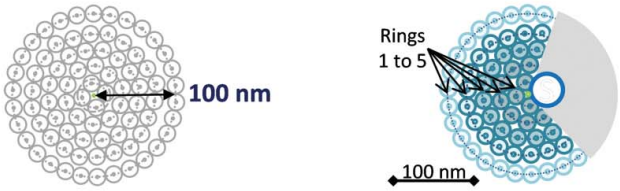

Ring	CaV_R	*d* nm	Ca_i µM	CaV $P_{o=}0.2$	ΣCaV*Ca_i µM	CaV_i P_R	ΣCaV_i $P_{R\text{-}SD}$
5	20	100	6	4	152	<0.01	0
4	15	76	9	3		0.02	0
3	11	56	14	2.2		0.07	0.07
2	7	36	28	1.4		0.22	0.22
1	3	14	80	0.6		0.56	0.30
					P_R=0.73		$P_{R\text{-}SD}$ =0.59
$P_{R\text{-}SD}/P_R$: 81%					$1 \frac{N_E}{N_{MAX}}$		

B. Ca2+ nanodomain profiles with saturated (0) cytoplasmic buffer or 10 mM EGTA.

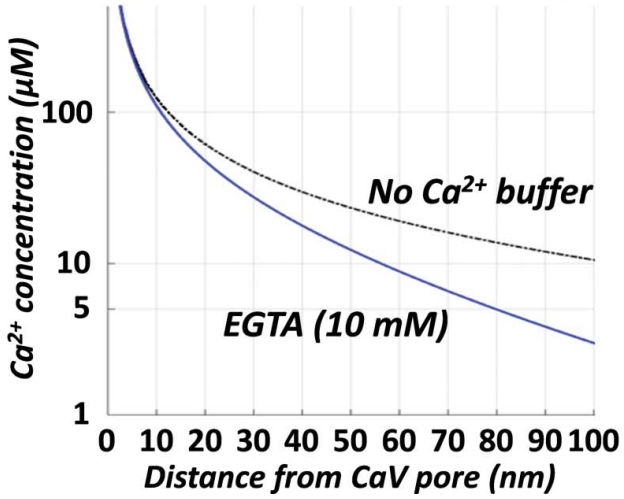

Figure 3. (**A**) Maximial release site. CaV density up to the 100 nm limit (*left diagram*) with an added 'Ca^{2+} shadow' due to the SV (*right diagram*). SVs were arranged in concentric rings at radii (*d*) centered on the SV-sensor and P_R and $P_{R\text{-}SD}$ were calculated as above (see adjoining Worksheet). Minor mathematical inconsistencies were introduced by rounding of values. (**B**) Ca^{2+} profiles calculated as in **Fig. 1** without Ca^{2+} buffer or in the presence of 10 mM EGTA (*as labeled*).

between Ca^{2+} and distance (**Fig. 1C**, *upper panel*) the calculated probability of release by the total Ca^{2+} from the 2 channels, P_R, is invariably higher than the sum of the probabilities from each channel alone, $P_{R\text{-}SD}$. Thus, the overall P_R reflects the sum of single domain gating by either channel alone plus an ***overlap-bonus***. With two channels abutting the SV-sensor the calculated overlap-bonus is modest, only ~14% (*worksheet not shown, see the following for a similar example*). Up to 3 channels can be positioned equidistant from the SV-sensor if their pores are located slightly further away (~14 nm **Fig. 2C**) and yields an overall P_R value of 0.39. The sum of the probability that the SV-sensor is activated by each channel alone (as for **Fig. 2B**, *left 2 panels*) gives $P_{R\text{-}SD}$ of 0.34 and the $P_{R\text{-}SD}/P_R$ ratio is 86%. Thus, N_E must be close to its minimum value while there was no significant increase in the overlap-bonus as compared to 2 channels.

Maximal calcium channel density release site

While the **Mini-CaV** models serve as a basic model for many synapses they cannot readily explain release site gating at synapses with release probability higher than 0.4.[55,56] To explore the upper limit to release site gating we clustered CaVs in a near-crystalline array up to a 100 nm radius from the SV-sensor (**Maxi-CaV** model, **Fig. 3**). The 100 nm limit was set as the maximal diffusion distance for the onset of release gating (~0.2 ms).[5,57] This is, however, a compromise distance. More distant channels could participate if ions that arrive later than 0.2 ms contribute significantly to fast release, or the limiting distance could be shorter if a significant fraction of the measured 0.2 ms delay arises from events downstream of SV-sensor activation.[4] Such cases are known to occur at biological synapses (*for example, see* Mossy Fiber synapse *below*) but do not appear to be typical of fast transmitting synapses and are beyond the main scope of our discussion.

A 100 nm circle can accommodate as many as 82, 20 nm channels in 5 concentric rings (**Fig. 3A**, *left diagram*). However, a 'diffusion-shadow' created by the SV itself is likely to occlude ion flux from a fraction of channels (**Fig. 3A**, *right diagram*).[58] The calculated P_R for this model (**Fig. 3A**, *worksheet*), 0.73, is sufficiently high to account for reported values at almost all synapses. It is also likely to be underestimated as we have not included 2 factors: some of the Ca^{2+} from the occluded channels in the diffusion shadow will undoubtedly reach the SV=sensor and also we have not factored in 'buffer saturation' which is likely to be significant

in this model. Even with a low CaV *Po*, there is significant probability that 2 or more CaVs open at the same time. Buffer saturation can be described simply as when 2 channels open at the same time their nanodomain profiles will be expected to increase because the accumulated Ca^{2+} more effectively saturates cytoplasmic buffers. To determine the scope of the calculation error we estimated the maximum possible effect of buffer saturation on P_R by simply recalculating P_R using a CaV nanodomain profile generated without *any* cytoplasmic buffer (**Fig. 3B**) - thus, simulating 100% buffer saturation. Interestingly, as noted previously,[59] as the mobile cytoplasmic buffer concentration is low this had a minor effect on the nanodomain profile, and the calculated P_R increased very little, to 0.76 (*worksheet not shown*). Thus, the $P_{R\text{-}SD}/P_R$ ratio, with or without cytoplasmic buffer saturation (81 and 78%, respectively), predicts an N_E value closer to 1 than N_{MAX}. Hence, we conclude that single domain-based release dominates even at the **Maxi-CaV** model synapse.

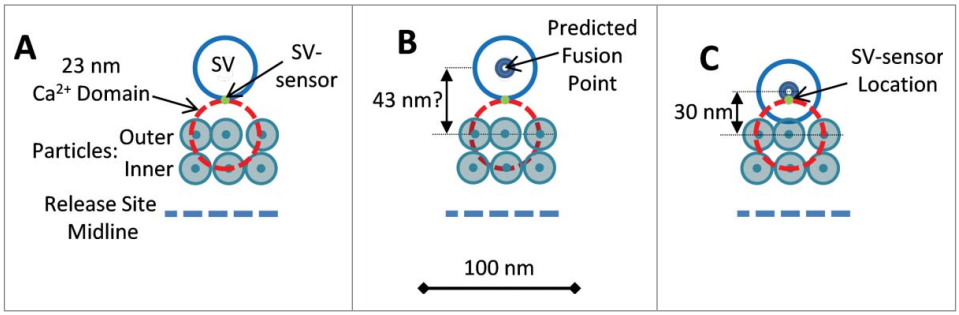

Figure 4. (**A**) Scale diagrams of frog NMJ release sites showing one pair of particle rows (as in freeze-fracture images; a second pair is located on the other side of the mid-line)[89] with an adjoining SV with its SV-sensor (assumed initially to be on the leading edge of the SV). The CaV that gates fusion is presumed to be the closest particle[38] and is shown with a 23 nm circle (*orange dashed line*) corresponding to the calculated CaV pore to SV-sensor distance (*see text*). (**B**) Based on the structural model in (**A**) the SV fusion point is predicted to be 43 nm from the CaV pore. (**C**) Structural model with the corrected SV fusion point at 30 nm from the outer particle row (*see text*). The SV-sensor was relocated to maintain a CaV pore-to SV sensor distance of 23 nm.

Release site gating at nerve terminals

Frog neuromuscular junction

Since transmitter release is by single domains at this synapse $P_{R\text{-}SD}$ must be equal to the experimentally determined P_R, 0.06[38] (and also as modeled in the **Mini-CaV** release site model, **Fig. 2A**). This value was used together with the published CaV *Po*, 0.16,[37] to back-calculate (**Equation 1**, **Fig. 1**, *lower panel*) a CaV to SV-sensor distance of 23 nm. The single CaV that gates release can be reasonably presumed to be located in the outer of the double particle rows in freeze fracture images, abutting the SV.[38] We used this distance to predict the location of the SV sensor on the SV. We started with the assumption that the SV-sensor is located on the leading-edge of the SV, facing the channel, but at the same plane as the surface membrane (**Fig. 4A**). With this model the SV fusion point (assumed to be in its center) should be 43 nm (that is 23 nm plus the SV radius, 20 nm) from the outer row membrane particle (**Fig. 4B**). However, this is a longer distance than measured in freeze fracture replicas[34]: ~30 nm from the outer particle array (**Fig. 4C**)[60]. Thus, the SV-sensor cannot be located on the edge of the SV but must be further toward its center. The data can be reconciled if the SV-sensor is relocated near the center of the SV, in essence abutting its fusion machinery (**Fig. 4D**).

Calyx of Held

Graphic modeling was used to explore SV gating using published calyx of Held data (**Introduction, Table 1**). EGTA block was simulated using an appropriate CaV domain concentration profile (**Fig. 3B**) and a similar worksheet analysis strategy (*not shown*). Although a mean of ~12 CaV gold particles was localized to each putative release site (*see* **Introduction**), these could be distributed over a relatively large area and hence, individual SVs might only be in 'range' of a subset of these CaVs. Thus, in our analysis below we explore gating with 6 channels. The SVs were reported to abut the CaV clusters, ~19 nm from the closest channel. Thus, the calyx of Held release site can reasonably be considered as intermediary between the **Mini-CaV**, and **Maxi-CaV** release site models above. However, the structural data for the calyx of Held can only be used as a starting point for modeling since incomplete labeling and analysis methods leave uncertainties in the actual number or distribution of the channels.[52] Nonetheless, putative models, as below, provide meaningful insight into the release physiology at the molecular level.

Various arrangements of 6 CaVs were tested to illustrate release at this synapse. With only one CaV abutting the SV-sensor and the others located at varying distances up to 80 nm away, the calculated release parameters were consistent with experimental findings (**Fig. 5B; Table 1**). With two channels abutting the SV sensor the release probability increased but other parameters remained similar (**Fig. 5C**). However, numerous modeling attempts in which there was at least one channel within 19 nm of the SV-sensor invariably resulted in a high $P_{R\text{-}SD}/P_R$ ratio, a low to moderate EGTA sensitivity and low N_E values. Interestingly, if the nearest channels of the cluster were located a moderate distance further away P_R declined markedly, and EGTA sensitivity increased, as expected, but the $P_{R\text{-}SD}/P_R$ ratio *increased* as the SV-sensor remained within range of the closest CaV nanodomains.

Neonatal calyx of Held

We next tested if graphic modeling could reproduce the high EGTA sensitivity and CaV titration N values at the pre-hearing neonatal calyx of Held, attributed to remote CaVs. While the single action potential-gated P_R has been reported as two to three-fold higher in the neonate than adult[45,47,61] this is due to longer

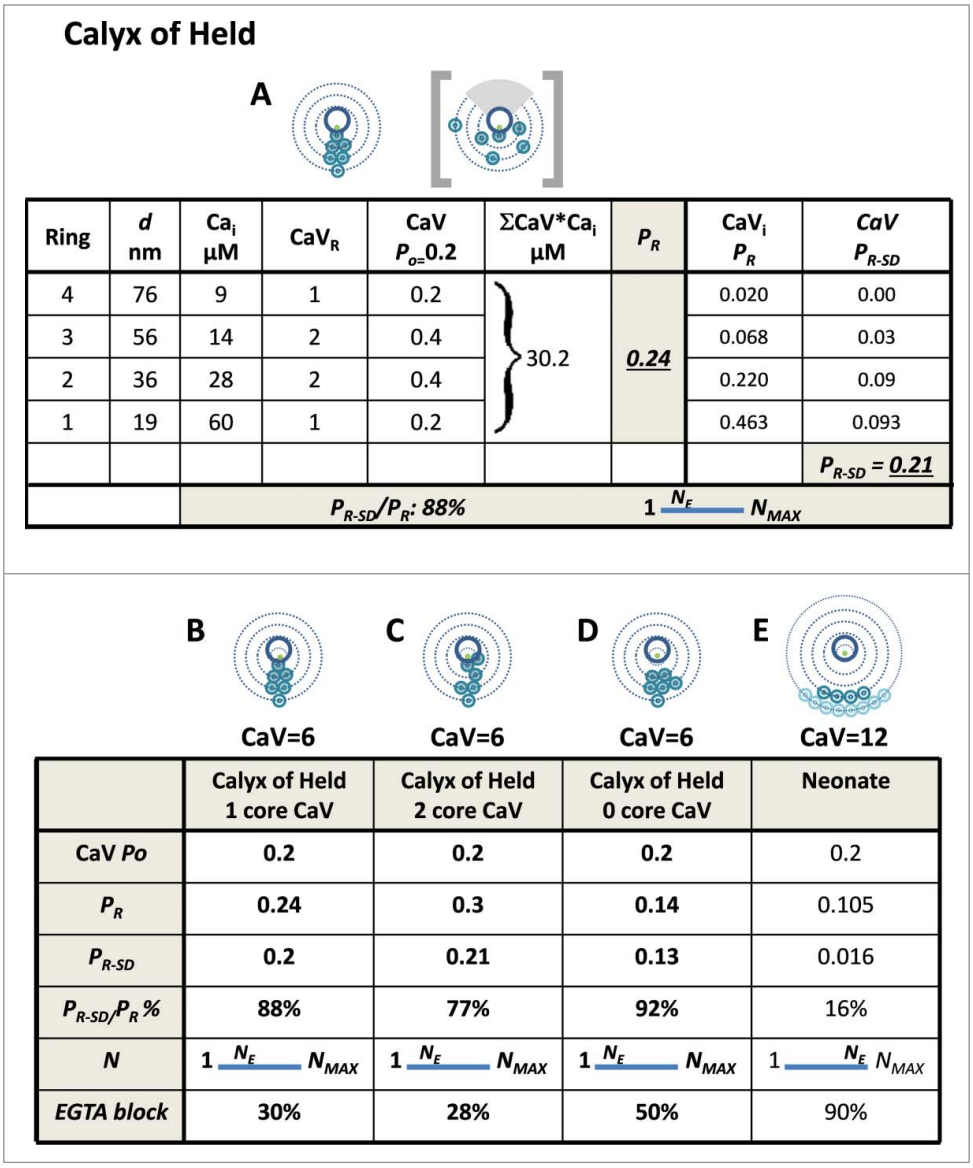

Ring	d nm	Ca_i µM	CaV_R	CaV $P_{o=}0.2$	ΣCaV*Ca_i µM	P_R	CaV_i P_R	CaV $P_{R\text{-}SD}$
4	76	9	1	0.2	30.2	0.24	0.020	0.00
3	56	14	2	0.4			0.068	0.03
2	36	28	2	0.4			0.220	0.09
1	19	60	1	0.2			0.463	0.093
								$P_{R\text{-}SD}$ = 0.21
	$P_{R\text{-}SD}/P_R$: 88%					$1 \frac{N_E}{} N_{MAX}$		

	Calyx of Held 1 core CaV	Calyx of Held 2 core CaV	Calyx of Held 0 core CaV	Neonate
CaV *Po*	0.2	0.2	0.2	0.2
P_R	0.24	0.3	0.14	0.105
$P_{R\text{-}SD}$	0.2	0.21	0.13	0.016
$P_{R\text{-}SD}/P_R$ %	88%	77%	92%	16%
N	$1 \frac{N_E}{} N_{MAX}$	$1 \frac{N_E}{} N_{MAX}$	$1 \frac{N_E}{} N_{MAX}$	$1 \frac{N_E}{} N_{MAX}$
EGTA block	30%	28%	50%	90%

Figure 5. *Graphic model of the release sites based on the calyx of Held.* A-D. *Release site with 6 calcium channels.* (**A**) Channels arranged at various distances from the SV sensor up to 80 nm (*see* **Fig. 2B** for model strategy). The distance from the channel to the SV-sensor is the key factor in the model; thus, the channels could be located at any point on their respective ring, excluding the gray SV shadow region as in the box-bracket example). Worksheet calculation of P_R and $P_{R\text{-}SD}$, predicting a low N_E value. (**B**) Summary of data in **A**. (**C**) As in **A**, with 2 CaVs in the inner Ring 1 (one CaV was moved to Ring 1 from Ring 2). (**D**) As in **A**, but with no CaVs in the inner Ring 1 (one CaV was moved from Ring 1 to Ring 3). (**E**) Simulation of release site function at the neonate calyx of Held with all the CaVs located remote from the SV-sensor (Rings 4 and 5). The model predicts a high N_E value and high block by EGTA, consistent with experimental findings (**Table 1**).

duration action potentials in the young animal and not a higher release efficiency.[57] Gleaning from a study in which voltage clamp pulses were used to trigger release rather than native action potentials[57] we estimate that with similar action potential durations the neonate P_R is approximately half the mature value, and hence ~0.1 (**Table 1**).

The calculated P_R value was invariably too low with a 7 channel CaV2.1 cluster[52] located sufficiently far from the SV-sensor (80 and 100 nm Rings) to simulate the *N* and EGTA sensitivity values (*not shown*). However, addition of 5 additional CaVs, to allow for additional neonatal CaV2.2 and CaV2.3 channels[52,62] provided a satisfactory estimate (**Fig. 5E**) and is at least consistent with a distant-CaVs hypothesis at the immature calyx. Interestingly, in the presence of high EGTA the graphic modeling method predicted a reduction of the CaV-titration test *N* value (*worksheet not shown*), consistent with published findings (**Table 1**). This finding is attractive since it implies that a steepening of the nanodomain profile by the buffer (**Fig. 3B**) increases the dependence of release on CaV single domains.

Discussion

Several themes emerge from the above analyses. First, a single, close CaV can generate a sufficiently high P_R to account for SV fusion at many synapses.[38,55] Even with a large field of densely packed CaVs, those closest to the SV-sensor play the primary role in release gating and their addition or removal dramatically alters the overall P_R (**Figs. 2D, 5**). Interestingly, single domain-based secretion is not limited to the very closest CaVs: channels that are as remote as 50 nm from the SV-sensor (**Fig. 2D**, *Ring 3*) can also make a significant contribution.[19]

The graphic modeling method omits several parameters included in previous models as they are not critical for the purposes of this report except under particular circumstances (*see also below*). These include synapse-specific Ca^{2+} buffering; the stochastic nature of single CaV kinetics, and variations in SV-sensor properties. These parameters have been discussed and modeled elsewhere[4,5,12,32,41,52,59,63-66] but even the most mathematically sophisticated models remain subject to limitations arising from release site architecture unknowns and the specific properties of CaVs and SV-sensors. Thus, despite their detail and sophistication, such models do not necessarily result in a consensus; an example pertinent to the present report is that release sites with a

short CaV to SV sensor distance have been argued to favor single,[26] and also the opposite, overlapping[52] domain-based release. While, graphic modeling is mathematically unsophisticated by comparison, its transparency, flexibility and simplicity provides significant advantages with respect to the primary issues addressed in this study.

Calculating the effect of buffer saturation is a significant challenge for all release site models. The calcium domain profile was modeled including a low concentration, fast on-rate buffer, as in previous studies.[30,31] Simply put, if the opening of 2 nearby channels coincide, the nanodomain generated by a second channel would be predicted to be more extensive due to saturation of cytoplasmic Ca^{2+} scavengers by the ions that enter through the first channel.[19] Such effects can be calculated with reasonable confidence for the averaged Ca^{2+} influx from many relatively remote channels.[12,19] However, when the CaVs are relatively close to the SV-sensor, the degree of buffer saturation is likely to depend on the precise molecular architecture – which is unique for each release site. Previous models have generally circumvented this issue by arranging the channels in mathematically tractable, but in essence non-biological, patterns[26,52] or by mathematical simplifications or assumptions.[19,32]

For several reasons we omitted buffer saturation from most of our calculations. First, the error is unlikely to be large as with typical biological low cytoplasmic buffer concentrations the nanodomain profile is dictated primarily by diffusion.[67] Second, as mentioned above, mathematical calculation may introduce more errors than it solves because release sites with multiple CaVs located at defined distances from the SV-sensor have virtually an infinite number of unique arrangements (e.g **Fig. 5A**, *square bracket diagram*). Third, buffer saturation should be minor at the **Mini-Channel** model and the frog NMJ, as the number of CaVs at the release site and their ***Po*** values are both low and hence, domain overlap can be predicted to be rare. As addressed in the Results section, because of the high number of channels, buffer saturation can be expected to be a factor for the **Maxi-channel** model (**Fig. 3A**). To test if this might have a significant effect on our calculations we repeated the simulations assuming 100% buffer saturation. The minimal effect on the calculated P_R argues that buffer saturation does not alter the qualitative interpretation of any of our models. Obviously, if the amount or on-rates of the native buffer was grossly underestimated then our predicted values would be too low – but this would introduce other contrary effects, including a reduction in release gated by remote channels with single impulses that might prove difficult to reconcile.

As discussed in the **Introduction**, single domain-based release gating predominates at most, if not all, fast-transmitting synapses studied to date. Since individual CaVs have a relatively low probability of opening during an action potential this organization may seem counterintuitive. However, it may have several functional advantages. First, it ensures that only a small fraction of release-ready SVs will be released during each action potential, protecting against premature exhaustion at a synapse where reliability is paramount – such as the NMJ. A second advantage is temporal: the wider the scatter of the CaVs, the greater the variability in SV gating latency and the lower the fidelity of impulse transmission, a factor that may be important in many neural processes. Third, single channel gating is highly efficient as the small Ca^{2+} influx both minimizes the amount of energy required for ion extrusion and any cross talk between the transmitter release machinery and other Ca^{2+}-dependent processes. Gating of release by single channels has major consequences on release physiology, in particular if a small fraction of channels are activated, as with a typical action potential. Then the steep, 4^{th} or 5th power relationship between Ca^{2+} and SV-sensor activation serves to minimize release by microdomains whereas an individual CaV nanodomain will trigger SV discharge.

It should be noted that the conclusions above may only apply to fast-transmitting synapses. The hippocampal mossy fiber synapse provides a fascinating contrast. Transmitter release at this synapse is highly sensitive to the EGTA block test, arguing for overlapping domain-gated release and predicting a long, ~70 nm, CaVs to SV-sensor separation.[68] However, this mossy fiber synapse also exhibits very different physiological properties with, perhaps, closer similarities to neurosecretory cells[69] than fast-transmitting synapses. These properties include extreme facilitation during a stimulus train, long synaptic delays and release durations, and a low SV-sensor *n* value of less than 2.[68] It is interesting to speculate that the SV sensor at these synapses have a lower Ca^{2+} unbinding rate, permitting greater accumulation of bound ions and, hence, also input from more CaVs located much further afield than the 100 nm limit used in our models. Thus, there may be 2 fundamentally distinct release site types.[68] First, classical fast-sites designed for temporally-accurate information coding where SV release is controlled by intimately associated CaVs and single domains,[13,17,23,24,26,28,37] and facilitating sites at which temporal precision takes second place to transmitter release amplitude gradation[68] and gradation of release amplitude[68] and at which release is gated by the smoothly graded overlapping domains of distant CaVs. This also raises the intriguing possibility that the latter, overlapping-domain/slow release site is an intermediary stage in the development of the fast, single domain dominated sites.[50,70] According to this hypothesis, transmitter release initially contributes to synapse formation[71] before adapting for fast information transfer. This idea might explain the pronounced release physiology switch, corresponding to the onset of hearing, during development from the neonatal to mature calyx of Held.

Numerous studies have concluded that at classical fast transmitting excitatory and inhibitory synapses the SV-sensor is located within 25 nm from the nearest CaV.[17,25, 52,72-74], but see: [75] As predicted,[17] this organizational precision argues for a linking molecular 'tether' and is supported by both structural[76-78] and biochemical[79-82] evidence. However, the protein composition of the tether apparatus, and whether it links directly to the CaV[80] or via a bridging molecule[81] remains to be determined. The localization of the SV-sensor at the SV fusion point (**Fig. 4D**) is an additional clue to the nature of the tethering mechanism by further constricting predictions on its length, to ~40 nm. This prediction also provides

support for the tacit assumption in the field that the SV-sensor is an integral element of the fusion apparatus.

Methods

Calcium channel domain and SV-sensor activation. The CaV domain was based on an inward current 0.33 pA (CaV2.2 channel; −65 mV, as during the repolarization phase of the action potential) entering an unbounded cytoplasmic space with a mobile Ca^{2+} 1 μM-affinity buffer at 50 μM concentration.[30] In simulations with cytoplasmic EGTA (10 mM) the domain profile was recalculated using appropriate binding constants. The SV-sensor was modeled with 5 equal and independent binding sites, each with a 10 μM binding affinity[3] (see[30]) and the P_R was calculated as detailed in **Fig. 1** (*lower panel*). Note summed single domain release probabilities were corrected for SV depletion.

Graphic modeling assumptions and simplifications

The basic approach to release gating using Graphic modeling is similar to that described previously.[19]

Graphic modeling is based on the following assumptions

#1. Presynaptic release-site associated CaVs are treated as a single CaV2 family type. The calcium domain profile establishes instantaneously and is determined by the current through the channel pore, free diffusion and 50 μM of fast buffer as 'normal' (**Fig. 1C**). CaV openings are sufficient to establish equilibrium binding to the SV sensor with an open probability (***Po***) of 0.2.[84] While CaV kinetics at different synapses are undoubtedly important,[85] here they are kept constant to permit release site organization comparisons.

#2. The docked and primed SV has a single active Ca^{2+} sensor aligned toward the channel[30,58] and fuses upon occupation of its 5 independent, 10 μM affinity, Ca^{2+} binding sites.[3] This model is used as it was developed using brief, action potential-like Ca^{2+} transients; it is consistent with other studies and models,[24,59,67,86] and also for its mathematical simplicity. SV release probabilities were calculated as in **Fig. 1** (lower panel).[30,87]

#3. Release site components are presumed to lie on a flat surface. The space on the surface membrane occupied by each CaVs is an important variable for packing density. Direct measurement of CaV2.2 distribution on a fixed, but hydrated calyx nerve terminal transmitter release face[88] and quantitative measurements of inter-membrane particle distances at the freeze-fractured frog neuromuscular junction replicas[89] gave inter-channel distances of ~17 nm. A recent report carried out a similar analysis on presynaptic CaV2.1 channels identified in a freeze-fracture replica by immunogold and reported a minimal 20 nm separation.[52] We have used the latter value in these simulations, presuming that each channel occupies a 20 nm diameter circular space. The SV is modeled as a sphere with a 40 nm diameter.

Disclosure of Potential Conflicts of Interest

No potential conflicts of interest were disclosed.

Acknowledgments

I thank Victor Matveev for Ca^{2+} concentration nanodomain simulations. I also thank Victor and David DiGregorio for critique on an earlier version of the manuscript and Sabiha Gardezi, Robert Chen, Arup Nath and Brittany Elliott for discussion and comments.

Funding

This work was supported by Canadian Institute of Health Science awards 86588 and 133602 and a Canada Research Chair.

References

1. Dodge FA Jr, Rahamimoff R. Co-operative action of calcium ions in transmitter release at the neuromuscular junction. J Physiol (Lond.) 1967; 193:419-32; PMID:6065887; http://dx.doi.org/10.1113/jphysiol.1967.sp008367
2. Stanley EF. Decline in calcium cooperativity as the basis of facilitation at the squid giant synapse. J Neurosci 1986; 6:782-9; PMID:2870141
3. Bollmann JH, Sakmann B, Borst JG. Calcium sensitivity of glutamate release in a calyx-type terminal. Science 2000; 289:953-7; PMID:10937999; http://dx.doi.org/10.1126/science.289.5481.953
4. Bollmann JH, Sakmann B. Control of synaptic strength and timing by the release-site Ca^{2+} signal. Nat Neurosci 2005; 8, 426-34; PMID:15750590
5. Simon SM, Llinas RR. Compartmentalization of the submembrane calcium activity during calcium influx and its significance in transmitter release. Biophys J 1985; 48:485-98; PMID:2412607; http://dx.doi.org/10.1016/S0006-3495(85)83804-2
6. Zucker RS, Fogelson AL. Relationship between transmitter release and presynaptic calcium influx when calcium enters through discrete channels. Proc Natl Acad Sci U S A 1986; 83:3032-6; PMID:2422666; http://dx.doi.org/10.1073/pnas.83.9.3032
7. Schneggenburger R, Neher E. Intracellular calcium dependence of transmitter release rates at a fast central synapse. Nature(Lond.) 2000; 406:889-93; http://dx.doi.org/10.1038/35022702
8. Branco T, Staras K. The probability of neurotransmitter release: variability and feedback control at single synapses. Nat Rev Neurosci 2009; 10:373-83; PMID:19377502; http://dx.doi.org/10.1038/nrn2634
9. Llinas RR, Steinberg IZ, Walton K. Relationship between presynaptic calcium current and postsynaptic potential in squid giant synapse. Biophys J 1981; 33:323-51; PMID:6261850; http://dx.doi.org/10.1016/S0006-3495(81)84899-0
10. Chad JE, Eckert R. Calcium domains associated with individual channels can account for anomalous voltage relations of Ca-dependent responses. Biophys J 1984; 45:993-99; PMID:6329349; http://dx.doi.org/10.1016/S0006-3495(84)84244-7
11. Augustine GJ, Charlton MP. Calcium dependence of presynaptic calcium current and post-synaptic response at the squid giant synapse. J Physiol (Lond.) 1986; 381:619-40; PMID:2442355; http://dx.doi.org/10.1113/jphysiol.1986.sp016347
12. Fogelson AL, Zucker RS. Presynaptic calcium diffusion from various arrays of single channels. Biophys J 1985; 48:1003-7; PMID:2418887; http://dx.doi.org/10.1016/S0006-3495(85)83863-7
13. Yoshikami D, Bagaboldo Z, Olivera BM. The inhibitory effects of omega-conotoxins on Ca channel and synapses. Ann N Y Acad Sci 1989; 560:230-48; PMID:2545135; http://dx.doi.org/10.1111/j.1749-6632.1989.tb24100.x
14. Augustine GJ. Regulation of transmitter release at the squid giant synapse by presynaptic delayed rectifier potassium current. J Physiol (Lond.) 1990; 431:343-64; PMID:1983120; http://dx.doi.org/10.1113/jphysiol.1990.sp018333
15. Adler EM, Augustine GJ, Duffy SN, Charlton MP. Alien intracellular calcium chelators attenuate neurotransmitter release at the squid giant synapse. J Neurosci 1991; 11, 1496-507; PMID:1675264
16. Augustine GJ, Adler EM, Charlton MP. The calcium signal for transmitter secretion from presynaptic nerve terminals. Ann NY Acad Sci 1991; 635:365-81; http://dx.doi.org/10.1111/j.1749-6632.1991.tb36505.x
17. Stanley EF. Single calcium channels and acetylcholine release at a presynaptic nerve terminal. Neuron 1993; 11:1007-11; PMID:8274272; http://dx.doi.org/10.1016/0896-6273(93)90214-C
18. Matveev V, Bertram R, Sherman A. Calcium cooperativity of exocytosis as a measure of Ca(2)+ channel domain overlap. Brain Res 2011; 1398:126-38; PMID:21621748
19. Bertram R, Smith GD, Sherman A. Modeling study of the effects of overlapping Ca^{2+} microdomains on neurotransmitter release. Biophys J 1999; 76:735-50; PMID:9929478; http://dx.doi.org/10.1016/S0006-3495(99)77240-1

20. Mulligan SJ, Davison I, Delaney KR. Mitral cell presynaptic Ca(2+) influx and synaptic transmission in frog amygdala. Neuroscience 2001; 104:137-51; PMID:11311538; http://dx.doi.org/10.1016/S0306-4522(01)00057-4
21. Wachman ES, Poage RE, Stiles JR, Farkas DL, Meriney SD. Spatial distribution of calcium entry evoked by single action potentials within the presynaptic active zone. J Neurosci 2004; 24:2877-85; PMID:15044526; http://dx.doi.org/10.1523/JNEUROSCI.1660-03.2004
22. Gentile L, Stanley EF. A unified model of presynaptic release site gating by calcium channel domains. Eur J Neurosci 2005; 21:278-82; PMID:15654866; http://dx.doi.org/10.1111/j.1460-9568.2004.03841.x
23. Brandt A, Khimich D, Moser T. Few CaV1.3 channels regulate the exocytosis of a synaptic vesicle at the hair cell ribbon synapse. J Neurosci 2005; 25:11577-85; PMID:16354915; http://dx.doi.org/10.1523/JNEUROSCI.3411-05.2005
24. Shahrezaei V, Cao A, Delaney KR. Ca^{2+} from one or two channels controls fusion of a single vesicle at the frog neuromuscular junction. J Neurosci 2006; 26:13240-9; PMID:17182774; http://dx.doi.org/10.1523/JNEUROSCI.1418-06.2006
25. Eggermann E, Bucurenciu I, Goswami SP, Jonas P. Nanodomain coupling between Ca(2) channels and sensors of exocytosis at fast mammalian synapses. Nat Rev Neurosci 2011; 13:7-21; PMID:22183436; http://dx.doi.org/10.1038/nrn3125
26. Bucurenciu I, Kulik A, Schwaller B, Frotscher M, Jonas P. Nanodomain coupling between Ca^{2+} channels and Ca^{2+} sensors promotes fast and efficient transmitter release at a cortical GABAergic synapse. Neuron 2008; 57:536-45; PMID:18304483; http://dx.doi.org/10.1016/j.neuron.2007.12.026
27. Scimemi A, Diamond JS. The number and organization of Ca^{2+} channels in the active zone shapes neurotransmitter release from Schaffer collateral synapses. J Neurosci 2012; 32:18157-76; PMID:23238730; http://dx.doi.org/10.1523/JNEUROSCI.3827-12.2012
28. Kim MH, Li GL, Von Gersdorff H. Single Ca^{2+} channels and exocytosis at sensory synapses. J Physiol 2013; 591:3167-78; PMID:23459757; http://dx.doi.org/10.1113/jphysiol.2012.249482
29. Tarr TB, Dittrich M, Meriney SD. Are unreliable release mechanisms conserved from NMJ to CNS? Trends Neurosci 2013; 36:14-22; PMID:23102681; http://dx.doi.org/10.1016/j.tins.2012.09.009
30. Weber AM, Wong FK, Tufford AR, Schlichter LC, Matveev V, Stanley EF. N-type Ca^{2+} channels carry the largest current: implications for nanodomains and transmitter release. Nat Neurosci 2010; 13, 1348-50; PMID:20953196; http://dx.doi.org/10.1038/nn.2657
31. Naraghi M, Neher E. Linearized buffered Ca^{2+} diffusion in microdomains and its implications for calculation of $[Ca^{2+}]$ at the month of a calcium channel. J Neurosci 1997; 17:6961-73; PMID:9278532
32. Matveev V, Bertram R, Sherman A. Ca^{2+} current versus Ca^{2+} channel cooperativity of exocytosis. J Neurosci 2009; 29:12196-209; PMID:19793978; http://dx.doi.org/10.1523/JNEUROSCI.0263-09.2009
33. Robitaille R, Adler EM, Charlton MP. Strategic location of calcium channels at transmitter release sites of frog neuromuscular synapses. Neuron 1990; 5:773-9; PMID:1980068; http://dx.doi.org/10.1016/0896-6273(90)90336-E
34. Heuser JE, Reese TS, Landis DMD. Functional changes in frog neuromuscular junctions studied with freeze fracture. J Neurocytol 1974; 3, 109-31; PMID:4596345; http://dx.doi.org/10.1007/BF01111936
35. Pumplin DW, Reese TS, Llinas RR. Are the presynaptic membrane particles the calcium channels? Proc Natl Acad Sci U S A 1981; 78:7210-3; PMID:6273920; http://dx.doi.org/10.1073/pnas.78.11.7210
36. Venzin M, Sandri C, Akert K, Wyss UR. Membrane associated particles of the presynaptic active zone in rat spinal cord. A morphometric analysis. Bain Res 1977; 130:393-404.
37. Luo F, Dittrich M, Stiles JR, Meriney SD. Single-pixel optical fluctuation analysis of calcium channel function in active zones of motor nerve terminals. J Neurosci 2011; 31:11268-81; PMID:21813687; http://dx.doi.org/10.1523/JNEUROSCI.1394-11.2011
38. Luo F, Dittrich M, Cho S, Stiles JR, Meriney SD. Transmitter release is evoked with low probability predominately by calcium flux through single channel openings at the frog neuromuscular junction. J Neurophysiol 2015; 113(7):2480-9.
39. Stanley EF. The calcium channel and the organization of the presynaptic transmitter release face. TINS 1997; 20:404-9; PMID:9292969
40. Fedchyshyn MJ, Wang LY. Developmental transformation of the release modality at the calyx of held synapse. J Neurosci 2005; 25, 4131-40; PMID:15843616; http://dx.doi.org/10.1523/JNEUROSCI.0350-05.2005
41. Wang LY, Neher E, Taschenberger H. Synaptic vesicles in mature calyx of Held synapses sense higher nanodomain calcium concentrations during action potential-evoked glutamate release. J Neurosci 2008; 28:14450-8; PMID:19118179; http://dx.doi.org/10.1523/JNEUROSCI.4245-08.2008
42. Kochubey O, Han Y, Schneggenburger R. Developmental regulation of the intracellular Ca^{2+} sensitivity of vesicle fusion and Ca^{2+}-secretion coupling at the rat calyx of Held. J Physiol 2009; 587:3009-23; PMID:19403608; http://dx.doi.org/10.1113/jphysiol.2009.172387
43. Yamashita T, Eguchi K, Saitoh N, von GH, Takahashi T. Developmental shift to a mechanism of synaptic vesicle endocytosis requiring nanodomain Ca^{2+}. Nat Neurosci 2010; 13, 838-44; PMID:20562869; http://dx.doi.org/10.1038/nn.2576
44. Schneggenburger R, Han Y, Kochubey O. Ca(2+) channels and transmitter release at the active zone. Cell Calcium 2012; 52:199-207; PMID:22682961; http://dx.doi.org/10.1016/j.ceca.2012.04.011
45. Erazo-Fischer E, Striessnig J, Taschenberger H. The role of physiological afferent nerve activity during in vivo maturation of the calyx of Held synapse. J Neurosci 2007; 27, 1725-37; PMID:17301180; http://dx.doi.org/10.1523/JNEUROSCI.4116-06.2007
46. Yang YM, Wang LY. Amplitude and kinetics of action potential-evoked Ca^{2+} current and its efficacy in triggering transmitter release at the developing calyx of held synapse. J Neurosci 2006; 26, 5698-708; PMID:16723526; http://dx.doi.org/10.1523/JNEUROSCI.4889-05.2006
47. Iwasaki S, Takahashi T. Developmental regulation of transmitter release at the calyx of Held in rat auditory brainstem. J Physiol 2001; 534:861-71; PMID:11483715; http://dx.doi.org/10.1111/j.1469-7793.2001.00861.x
48. Jewett DL, Romano MN. Neonatal development of auditory system potentials averaged from the scalp of rat and cat. Brain Res 1972; 36:101-15; PMID:5008374; http://dx.doi.org/10.1016/0006-8993(72)90769-X
49. Borst JG, Sakmann B. Calcium influx and transmitter release in a fast CNS synapse. Nature(Lond.) 1996; 383:431-5; http://dx.doi.org/10.1038/383431a0
50. Fedchyshyn MJ, Wang LY. Activity-dependent changes in temporal components of neurotransmission at the juvenile mouse calyx of Held synapse. J Physiol 2007; 581:581-602; PMID:17347264; http://dx.doi.org/10.1113/jphysiol.2007.129833
51. Indriati DW, Kamasawa N, Matsui K, Meredith AL, Watanabe M, Shigemoto R. Quantitative localization of Cav2.1 (P/Q-type) voltage-dependent calcium channels in Purkinje cells: somatodendritic gradient and distinct somatic coclustering with calcium-activated potassium channels. J Neurosci 2013; 33:3668-78; PMID:23426693; http://dx.doi.org/10.1523/JNEUROSCI.2921-12.2013
52. Nakamura Y, Harada H, Kamasawa N, Matsui K, Rothman JS, Shigemoto R, Silver RA, DiGregorio DA, Takahashi T. Nanoscale distribution of presynaptic Ca (2+) channels and its impact on vesicular release during development. Neuron 2015; 85:145-58; PMID:25533484; http://dx.doi.org/10.1016/j.neuron.2014.11.019
53. Stanley EF. Presynaptic calcium channels and the transmitter release mechanism. Ann N Y Acad Sci 1993; 681:368-72; PMID:8102841; http://dx.doi.org/10.1111/j.1749-6632.1993.tb22915.x
54. Sheng J, He L, Zheng H, Xue L, Luo F, Shin W, Sun T, Kuner T, Yue DT, Wu LG. Calcium-channel number critically influences synaptic strength and plasticity at the active zone. Nat Neurosci 2012; 15, 998-1006; PMID:22683682; http://dx.doi.org/10.1038/nn.3129
55. Thomson AM. Facilitation, augmentation and potentiation at central synapses. Trends Neurosci 2000; 23:305-12; PMID:10856940; http://dx.doi.org/10.1016/S0166-2236(00)01580-0
56. Gonzalez JC, Lignani G, Maroto M, Baldelli P, Hernandez-Guijo JM. Presynaptic muscarinic receptors reduce synaptic depression and facilitate its recovery at hippocampal GABAergic synapses. Cereb Cortex 2014; 24:1818-31; http://dx.doi.org/10.1093/cercor/bht032
57. Wang LY, Fedchyshyn MJ, Yang YM. Action potential evoked transmitter release in central synapses: insights from the developing calyx of Held. Mol Brain 2009; 2:36; PMID:19939269; http://dx.doi.org/10.1186/1756-6606-2-36
58. Shahrezaei V, Delaney KR. Consequences of Molecular-Level Ca^{2+} Channel and Synaptic Vesicle Colocalization for the Ca^{2+} Microdomain and Neurotransmitter Exocytosis: A Monte Carlo Study. Biophys J 2004; 87:2352-64; PMID:15454435; http://dx.doi.org/10.1529/biophysj.104.043380
59. Meinrenken CJ, Borst JG, Sakmann B. Local routes revisited: the space and time dependence of the Ca^{2+} signal for phasic transmitter release at the rat calyx of Held. J Physiol 2003; 547:665-89; PMID:12562955
60. Stanley EF. The calcium channel and the organization of the presynaptic transmitter release face. Trends Neurosci 1997; 20:404-9; PMID:9292969; http://dx.doi.org/10.1016/S0166-2236(97)01091-6
61. Koike-Tani M, Kanda T, Saitoh N, Yamashita T, Takahashi T. Involvement of AMPA receptor desensitization in short-term synaptic depression at the calyx of Held in developing rats. J Physiol 2008; 586:2263-75; http://dx.doi.org/10.1113/jphysiol.2007.142547
62. Iwasaki S, Takahashi T. Developmental changes in calcium channel types mediating synaptic transmission in rat auditory brainstem. J Physiol (Lond) 1998; 509:419-23; PMID:9575291; http://dx.doi.org/10.1111/j.1469-7793.1998.419bn.x
63. Matveev V. Calcium-Dependent Exocytosis, Biophysical Models of in Encyclopedia of Computational Neuroscience (eds. Jaeger D, Jung R) 1-17 (Springer New York, 2014).
64. Bennett MR, Farnell L, Gibson WG. The probability of quantal secretion within an array of calcium channels of an active zone. Biophys J 2000; 78:2222-40; PMID:10777722; http://dx.doi.org/10.1016/S0006-3495(00)76770-1
65. Bertram R, Sherman AD, Stanley EF. The single domain/bound calcium hypothesis of transmitter release and facilitation. J Neurophysiol 1996; 75:1919-31; PMID:8734591
66. Shahrezaei V, Delaney KR. Brevity of the Ca^{2+} microdomain and active zone geometry prevent Ca^{2+}-sensor saturation for neurotransmitter release. J Neurophysiol 2005; 94:1912-9; PMID:15888526; http://dx.doi.org/10.1152/jn.00256.2005
67. Meinrenken CJ, Borst JG, Sakmann B. Calcium secretion coupling at calyx of held governed by nonuniform channel-vesicle topography. J Neurosci 2002; 22:1648-67; PMID:11880495

68. Vyleta NP, Jonas P. Loose coupling between Ca^{2+} channels and release sensors at a plastic hippocampal synapse. Science 2014; 343:665-70; PMID:24503854; http://dx.doi.org/10.1126/science.1244811
69. Soldo BL, Giovannucci DR, Stuenkel EL, Moises HC. Ca(2+) and frequency dependence of exocytosis in isolated somata of magnocellular supraoptic neurones of the rat hypothalamus. J Physiol 2004; 555:699-711; PMID:14645448; http://dx.doi.org/10.1113/jphysiol.2003.051136
70. Baur D, Bornschein G, Althof D, Watanabe M, Kulik A, Eilers J, Schmidt H. Developmental tightening of cerebellar cortical synaptic influx-release coupling. J Neurosci 2015; 35:1858-71; PMID:25653347; http://dx.doi.org/10.1523/JNEUROSCI.2900-14.2015
71. Okawa H, Hoon M, Yoshimatsu T, Della SL, Wong RO. Illuminating the multifaceted roles of neurotransmission in shaping neuronal circuitry. Neuron 2014; 83:1303-18; PMID:25233313; http://dx.doi.org/10.1016/j.neuron.2014.08.029
72. Pangrsic T, Gabrielaitis M, Michanski S, Schwaller B, Wolf F, Strenzke N, Moser T. EF-hand protein Ca^{2+} buffers regulate Ca^{2+} influx and exocytosis in sensory hair cells. Proc Natl Acad Sci U S A 2015; 112, E1028-37; PMID:25691754; http://dx.doi.org/10.1073/pnas.1416424112
73. Schmidt H, Brachtendorf S, Arendt O, Hallermann S, Ishiyama S, Bornschein G, Gall D, Schiffmann SN, Heckmann M, Eilers J. Nanodomain coupling at an excitatory cortical synapse. Curr Biol 2013; 23:244-9; PMID:23273895; http://dx.doi.org/10.1016/j.cub.2012.12.007
74. Bucurenciu I, Bischofberger J, Jonas P. A small number of open Ca(2+) channels trigger transmitter release at a central GABAergic synapse. Nat Neurosci 2010; 13, 19-21; PMID:20010820; http://dx.doi.org/10.1038/nn.2461
75. Keller D, Babai N, Kochubey O, Han Y, Markram H, Schürmann F, Schneggenburger R. An Exclusion Zone for Ca^{2+} Channels around Docked Vesicles Explains Release Control by Multiple Channels at a CNS Synapse. PLoS Comput Biol 2015; 11:e1004253; PMID:25951120; http://dx.doi.org/10.1371/journal.pcbi.1004253
76. Harlow ML, Szule JA, Xu J, Jung JH, Marshall RM, McMahan UJ. Alignment of synaptic vesicle macromolecules with the macromolecules in active zone material that direct vesicle docking. PLoS ONE 2013; 8: e69410; PMID:23894473; http://dx.doi.org/10.1371/journal.pone.0069410
77. Nagwaney S, Harlow ML, Jung JH, Szule JA, Ress D, Xu J, Marshall RM, McMahan UJ. Macromolecular connections of active zone material to docked synaptic vesicles and presynaptic membrane at neuromuscular junctions of mouse. J Comp Neurol 2009; 513:457-68; PMID:19226520; http://dx.doi.org/10.1002/cne.21975
78. Harlow M, Ress D, Koster A, Marshall RM, Schwarz M, McMahan UJ. Dissection of active zones at the neuromuscular junction by EM tomography. J Physiol Paris 1998; 92:75-8; PMID:9782447; http://dx.doi.org/10.1016/S0928-4257(98)80141-1
79. Mochida S, Westenbroek RE, Yokoyama CT, Zhong H, Myers SJ, Scheuer T, Itoh K, Catterall WA. Requirement for the synaptic protein interaction site for reconstitution of synaptic transmission by P/Q-type calcium channels. Proc Natl Acad Sci U S A 2003; 100:2819-24; PMID:12601156; http://dx.doi.org/10.1073/pnas.262787699
80. Wong FK, Li Q, Stanley EF. Synaptic vesicle capture by CaV2.2 calcium channels. Front Cell Neurosci 2013; 7:101; PMID:23874268
81. Catterall WA. Interactions of presynaptic Ca^{2+} channels and snare proteins in neurotransmitter release. Ann N Y Acad Sci 1999; 868:144-59; PMID:10414292; http://dx.doi.org/10.1111/j.1749-6632.1999.tb11284.x
82. Sheng ZH, Westenbroek RE, Catterall WA. Physical link and functional coupling of presynaptic calcium channels and the synaptic vesicle docking/fusion machinery. J Bioenerg Biomembr 1998; 30, 335-45; PMID:9758330; http://dx.doi.org/10.1023/A:1021985521748
83. Llinas RR, Sugimori M, Simon SM. Transmission by presynaptic spike-like depolarization in the squid giant synapse. Proc Natl Acad Sci U S A 1982; 79:2415-9; PMID:6954549; http://dx.doi.org/10.1073/pnas.79.7.2415
84. Luvisetto S, Fellin T, Spagnolo M, Hivert B, Brust PF, Harpold MM, Stauderman KA, Williams ME, Pietrobon D. Modal gating of human CaV2.1 (P/Q-type) calcium channels: I. The slow and the fast gating modes and their modulation by β subunits. J Gen Physiol 2004; 124:445-61; PMID:15504896; http://dx.doi.org/10.1085/jgp.200409034
85. Stanley EF. PresyNaptic calcium channels: why is P selected before N? Biophys J 2015; 108:451-2; PMID:25650909; http://dx.doi.org/10.1016/j.bpj.2014.12.021
86. Ravin R, Parnas H, Spira ME, Volfovsky N, Parnas I. Simultaneous measurement of evoked release and $[Ca^{2+}]i$ in a crayfish release bouton reveals high affinity of release to Ca^{2+}. J Neurophysiol 1999; 81:634-42; PMID:10036266
87. Parnas H, Segel LA. A theoretical explanation for some effects of calcium on the facilitation of neurotransmitter release. J Theor Biol 1980; 84:3-29; PMID:6106090; http://dx.doi.org/10.1016/S0022-5193(80)81035-6
88. Haydon PG, Henderson E, Stanley EF. Localization of individual calcium channels at the release face of a presynaptic nerve terminal. Neuron 1994; 13:1275-80; PMID:7993621; http://dx.doi.org/10.1016/0896-6273(94)90414-6
89. Stanley EF, Reese TS, Wang GZ. Molecular scaffold reorganization at the transmitter release site with vesicle exocytosis or botulinum toxin C1. Eur J Neurosci 2003; 18:2403-7; PMID:14622203; http://dx.doi.org/10.1046/j.1460-9568.2003.02948.x